How to cite: Angew. Chem. Int. Ed. 2024, e202318461
doi.org/10.1002/anie.202318461

Heterogeneous Catalysis

Converting Glycerol into Valuable Trioses by $Cu^{\delta+}$-Single-Atom-Decorated WO_3 under Visible Light

Lunqiao Xiong[+], Zhounan Yu[+], Hongchen Cao, Weixiang Guan, Yang Su, Xiaoli Pan, Leilei Zhang, Xiaoyan Liu, Aiqin Wang, and Junwang Tang**

Abstract: Photocatalytic selective oxidation under visible light presents a promising approach for the sustainable transformation of biomass-derived wastes. However, achieving both high conversion and excellent selectivity poses a significant challenge. In this study, two valuable trioses, glyceraldehyde and dihydroxyacetone, are produced from glycerol over $Cu^{\delta+}$-decorated WO_3 photocatalyst in the presence of H_2O_2. The photocatalyst exhibits a remarkable five-fold increase in the conversion rate (3.81 $mmol \cdot g^{-1} \cdot h^{-1}$) while maintaining a high selectivity towards two trioses (46.4 % to glyceraldehyde and 32.9 % to dihydroxyacetone). Through a comprehensive analysis involving X-ray photoelectron spectroscopy measurements with and without light irradiation, electron spin resonance spectroscopy, and isotopic analysis, the critical role of Cu^+ species has been explored as efficient hole acceptors. These species facilitate charge transfer, promoting glycerol oxidation by photoholes, followed by coupling with OH^-, which are subsequently dehydrated to yield the desired glyceraldehyde and dihydroxyacetone.

Introduction

Harnessing solar energy to convert biowastes (e.g., CO_2) into useful compounds is a fundamental principle of nature. The emulation of this process using artificial means has been envisioned as an ideal approach to upgrade waste materials and address energy shortages. On the other hand, as the demand for energy continues to expand and environmental concerns gain more recognition, biodiesel is assuming an increasingly significant role in the global transportation sector.[1] This renewable fuel is derived from vegetable/animal oils and produces a substantial amount of glycerol as a by-product (10 kg of glycerol is generated from the production of 100 kg of biodiesel).[2] Strategic utilisation of glycerol can play a pivotal role in advancing biodiesel production and decreasing its overall cost, thereby leading the way towards a more environmentally sustainable future in the global transportation sector.[3] Within this context, there has been a considerable focus on the conversion of glycerol into high-value chemicals under visible light.[4] Glycerol has many oxidation derivatives, which not only endows it with significant potential for transformation into other valuable chemicals, but also makes selectivity control quite difficult.[5] Among the various derivatives, glyceraldehyde and dihydroxyacetone, two trioses, hold substantial applications in industries such as cosmetics, pharmaceuticals, and fine chemicals.[4a,6] The conversion of glycerol into glyceraldehyde and dihydroxyacetone thus presents an attractive market opportunity. Traditional thermocatalytic or electrocatalytic oxidation methods using noble metal catalysts such as Au, Ag, Pt, or Pd have been explored. However, these catalysts pose challenges due to their high cost, limited selectivity, and low production rates of the desired products.[7]

The utilisation of solar energy for light-driven photocatalytic glycerol oxidation offers an alternative pathway for converting biowaste into essential chemical building blocks.[8] Initial studies primarily focused on traditional TiO_2-based photocatalysts, extensively investigating parameters such as pH values, reactant concentration, and catalyst surface modification.[9] Another strategy employed to enhance catalytic activity and promote hydrogen production involved the incorporation of noble metals like Pt and Au, albeit at the expense of compromising selectivity toward valuable partial-oxidised products.[10] However, this tendency can be altered by employing different types of catalysts. For example, a comparison between the catalytic performance of commercial and home-prepared TiO_2 revealed differences in product distribution, with the highest selectivity achieved using Degussa P25 (13 % glyceraldehyde and 8 % dihydroxyacetone).[11] Subsequently, an in-depth exploration of the catalytic mechanism underlying the transformation of glycerol was conducted by analysing intermediate species formed as a function of glycerol concentration

[*] L. Xiong,[+] J. Tang
Department of Chemical Engineering, University College London, Torrington Place, London, WC1E 7JE, UK
E-mail: junwang.tang@ucl.ac.uk
Z. Yu,[+] H. Cao, W. Guan, Y. Su, X. Pan, L. Zhang, X. Liu, A. Wang
State Key Laboratory of Catalysis, Dalian Institute of Chemical Physics, Chinese Academy of Sciences, Dalian, 116023, China
E-mail: aqwang@dicp.ac.cn
J. Tang
Industrial Catalysis Center, Department of Chemical Engineering, Tsinghua University, Beijing 100084, China
[+] These authors contributed equally: Lunqiao Xiong, Zhounan Yu.

over TiO_2 powders. These studies have significantly advanced our understanding of glycerol photocatalytic oxidation over metal-oxide photocatalysts. However, while TiO_2 exhibits outstanding performance in absorbing light in the UV region, it lacks the ability to respond to visible light. Consequently, its practical application under sunlight is limited, as UV energy represents only a fraction (approximately 3–5 %) of the total solar energy reaching the Earth's surface.[12] Therefore, expanding the light absorption capacity of photocatalytic glycerol oxidation into the visible region is of paramount importance.

WO_3 presents excellent visible light responsiveness, standing as a highly promising metal-oxide photocatalyst. While extensively explored for applications such as pollutant degradation,[13] hydrogen production,[14] and energy storage,[15] its use in selective glycerol oxidation remains relatively uncommon due to its too strong oxidation potential. Moreover, although WO_3 exhibits some selectivity toward C_3 products, its conversion rate is rather moderate.[16] In this study, earth-abundant Cu species are atomically dispersed over the WO_3 surface by a highly reproducible method. The resulting photocatalyst exhibits remarkable efficiency in converting glycerol into glyceraldehyde and dihydroxyacetone under visible light irradiation, with a conversion rate of 3.81 $mmol \cdot g^{-1} \cdot h^{-1}$ and a high selectivity towards two trioses. Through various spectroscopic techniques, scavenging experiments, and isotopic studies, it has been revealed that the Cu^+ species act as hole acceptors, significantly enhancing charge transfer processes, and consequently boosting photocatalytic activity. Moreover, glycerol oxidation over $Cu^{\delta+}$-single-atom-decorated WO_3 proceeds via the activation of photogenerated holes, followed by the coupling with OH^-, and finally dehydrated into the target products.

Results and discussions

Cu cocatalyst was loaded onto the WO_3 surface using an impregnation method and is represented as xCu/WO_3, where×stands for the mass percentage of the loaded Cu species. The actual amount of Cu loaded was quantified using inductively coupled plasma atomic emission spectrometry (ICP-AES), very close to the nominal amount (Table S1). The structures of pristine WO_3 and Cu-loaded WO_3 were initially examined using X-ray diffraction (XRD), as depicted in Figure 1a. Following the introduction of Cu, WO_3 maintains its monoclinic structure, with no discernible diffraction peaks attributed to Cu or copper oxides observed. This is likely due to the low loading amount of Cu species or their high dispersion (Figure S1). The chemical states of the loaded Cu species were subsequently investigated using X-ray photoelectron spectroscopy (XPS). The peak at approximately 932 eV corresponds to Cu $2p_{3/2}$, while another peak at around 952 eV is associated with Cu $2p_{1/2}$ (Figure S2).[17] Both peaks can be resolved into two components, corresponding to Cu^+ and Cu^{2+} respectively. The high-resolution Cu LM2 Auger spectrum of $0.25Cu/WO_3$ further confirms that Cu^+ and Cu^{2+} coexist on the WO_3 surface, without the presence of Cu^0 (Figure S3). Additionally, the O 1s spectra indicate a decrease in the number of oxygen vacancies after loading the Cu species (Figure S4), supported by the presence of a defective layer observed on the catalyst surface (Figure S5).[18] The W 4f spectra for both WO_3 and $0.25\ Cu/WO_3$ exhibit three peaks at 41.5 eV, 37.9 eV and 35.7 eV, which can be ascribed to W^{6+} (Figure S6).[19]

The ultraviolet-visible (UV/Vis) spectrum of WO_3 exhibits a characteristic absorption band with an onset edge, indicative of a band gap of approximately 2.6 eV, consistent with widely reported values (Figure 1b).[16] The spectrum of the $0.25Cu/WO_3$ catalyst presents a similar light absorption capability with a slightly narrowed band gap of 2.4 eV. This reduction in band gap can be attributed to the insertion of Cu single atoms, as further analysed later. The morphology of $0.25Cu/WO_3$ was examined using transmission electron microscopy (TEM), as presented in Figure 1c. The WO_3 particles exhibit an average diameter of around 150 nm. At higher resolution (Figure 1d), the (200) crystalline fringes of WO_3 are observed. Importantly, no distinct particles are evident on $0.25Cu/WO_3$, while energy-dispersive X-ray (EDX) mapping shows a homogeneous distribution of Cu species (Figure S7 and Figure 1e), suggesting that Cu species are highly dispersed on the WO_3 surface.

The X-ray absorption near edge structure (XANES) curve of $0.25Cu/WO_3$ exhibits a higher K edge energy compared to Cu foil and Cu_2O, but slightly lower than that of CuO (Figure 1f and Figure S8, 9). All these confirm the presence of both Cu^+ and Cu^{2+} in $0.25Cu/WO_3$, which is consistent with the XPS results. Furthermore, the absence of a pre-edge peak suggests a disruption in the symmetry of the coordination environment and typical lattice structure, possibly due to the insertion of Cu into the WO_3 lattice. The Fourier transform extended X-ray absorption fine structure (FT-EXAFS) curves provide additional evidence for the single atom Cu structure in $0.25Cu/WO_3$, as there are no observable Cu–Cu or Cu–O–Cu peaks (Figure 1g). The shorter Cu–O peak in $0.25Cu/WO_3$ also indicates a distinct local structure for Cu. Fitting results presented in Table S2 reveal two Cu–O paths in this sample, with a total Cu–O coordination number less than 4. Notably, the shorter Cu–O1 path (1.68 Å) is close to W–O path (1.75 Å, mp-18773) rather than the Cu–O path (1.95 Å) in the CuO sample. This finding lends further support to the notion that a portion of Cu replaces W on the surface of WO_3.

Subsequently, pristine WO_3 samples and those loaded with Cu species were subjected to glycerol photocatalytic oxidation using hydrogen peroxide (H_2O_2) as an oxidant, with a glycerol to H_2O_2 ratio of 1:1. Pristine WO_3 shows a selectivity of 52.4 % towards glyceraldehyde and 33.8 % towards dihydroxyacetone, accompanied by a low conversion rate of 0.69 $mmol \cdot g^{-1} \cdot h^{-1}$ (Figure 2a). Two other liquid products, formic acid and glycolaldehyde, are generated in minimal quantities. The introduction of Cu species noticeably influences the catalytic performance of WO_3. Even with the addition of only 0.01% Cu species, the conversion rate increases to 1.88 $mmol \cdot g^{-1} \cdot h^{-1}$, displaying a selectivity of 56.8% towards glyceraldehyde and 31.7% towards dihydrox-

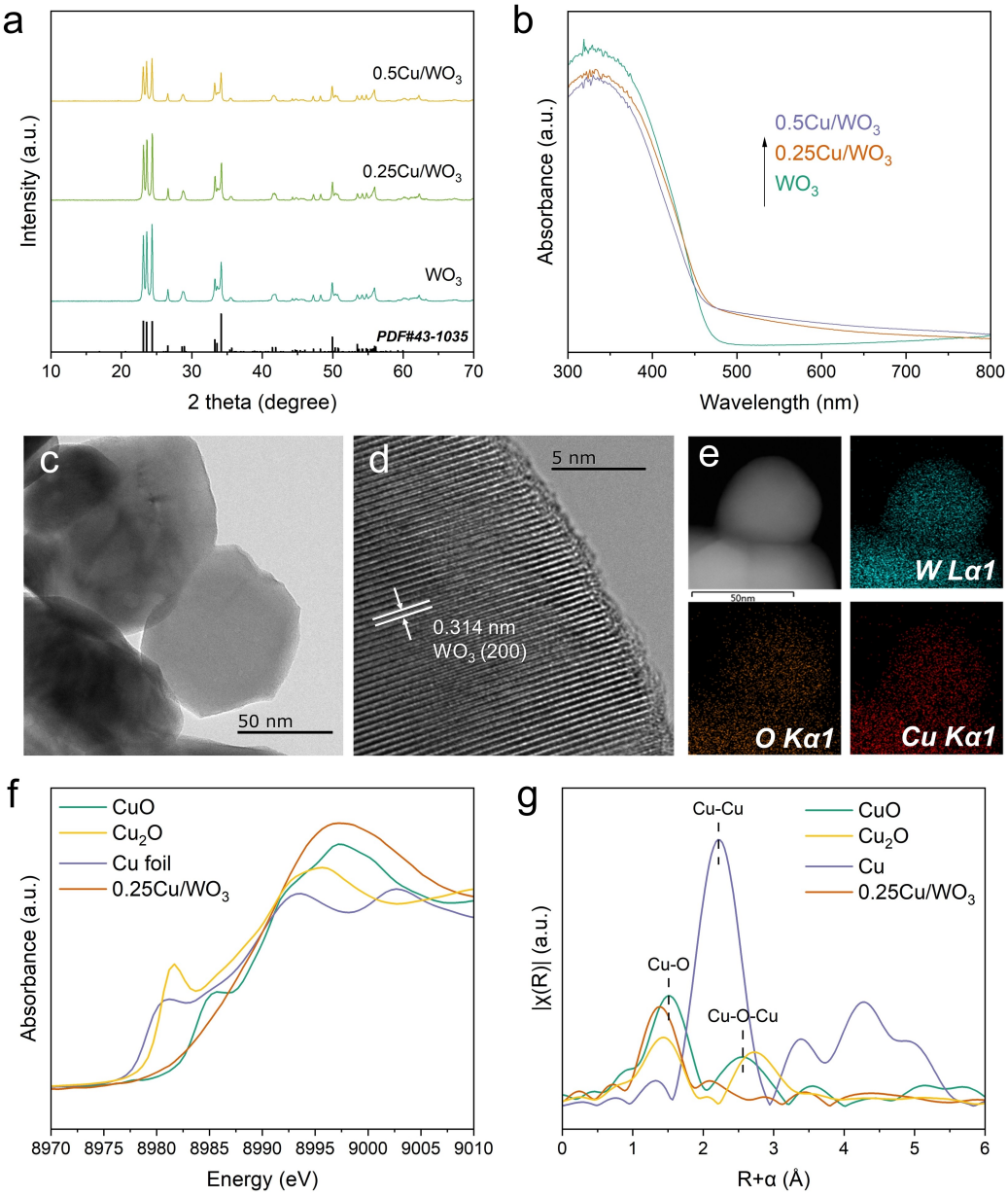

Figure 1. (a) XRD patterns and (b) UV/Vis spectra of WO_3, 0.25Cu/WO_3 and 0.5Cu/WO_3. (c) TEM image, (d) high-resolution TEM image and (e) EDX elemental mapping of 0.25Cu/WO_3. (f) Cu K-edge XANES spectra of the 0.25Cu/WO_3 catalyst and reference samples including copper foil, Cu_2O, and CuO. (g) FT-EXAFS spectra of the 0.25Cu/WO_3 catalyst and reference samples including copper foil, Cu_2O, and CuO.

yacetone. The most effective catalyst among the copper-species-loaded catalyst (0.25Cu/WO_3) exhibits a five-fold enhancement in the conversion rate (3.81 $mmol \cdot g^{-1} \cdot h^{-1}$) while maintaining a similar selectivity (46.4 % to glyceraldehyde and 32.9 % to dihydroxyacetone) compared to pristine WO_3. Further increasing the Cu loading slightly decreases the yield of liquid products.

To investigate the oxidation process, the temporal production of various products over 0.25Cu/WO_3 was recorded (Figure S10). All four products are generated at a relatively high rate during the initial hour, followed by a slowdown in the conversion rate over the subsequent three hours. Notably, the distribution of products remains unchanged despite variations in the conversion rate, with glyceraldehyde and dihydroxyacetone, two valuable chemicals, being the major products. Moreover, the H_2O_2 concentration plays a crucial role in enhancing the conversion rate, as depicted in Figure 2b. In the absence of H_2O_2, no glycerol conversion occurs. Increasing the H_2O_2 concentration improves the glycerol conversion rate, albeit with a slight decrease in selectivity towards glyceraldehyde and dihydroxyacetone. The enhancement in glycerol conversion attributed to the H_2O_2 concentration is relatively limited compared to the effect of increasing glycerol concentration, which linearly enhances the conversion rate (Figure S11).

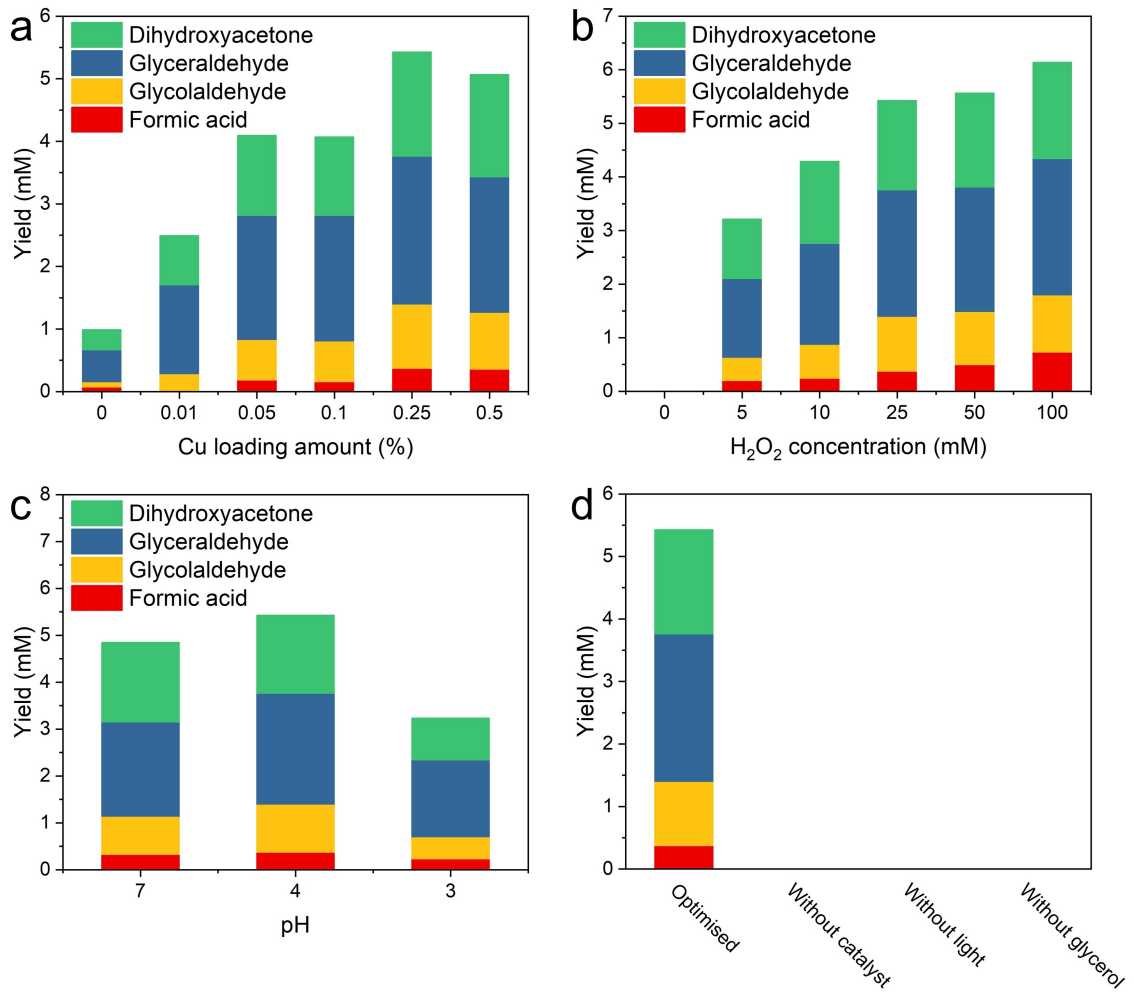

Figure 2. (a) The product distribution over Cu/WO_3 with different Cu loading amounts. (b) The product distribution over 0.25Cu/WO_3 with different H_2O_2 concentration. (c) The product distribution over 0.25Cu/WO_3 with different pH values. (d) Product yields from a series of control experiments. Reaction conditions: 10 mg catalyst, 30 mL of 25 mM glycerol aqueous solution with 25 mM H_2O_2, 25 °C, argon at atmospheric pressure, visible light irradiation (>420 nm), pH = 4 and 4 h reaction time unless otherwise specified.

The pH value of the reaction medium was optimised. Decreasing the pH from 7 to 4 through adding diluted H_2SO_4 solution results in an increase in the conversion rate from 3.54 $mmol \cdot g^{-1} \cdot h^{-1}$ to 3.81 $mmol \cdot g^{-1} \cdot h^{-1}$, potentially attributable to the reduced thermocatalytic decomposition rate of H_2O_2 (Figure 2c).[20] However, further decreasing the pH to 3 dramatically decreases the conversion rate to 2.32 $mmol \cdot g^{-1} \cdot h^{-1}$. This can be understood considering that WO_3 nanoparticles have an isoelectric point at around pH 2.[21] As the pH approaches this point, aggregation becomes increasingly severe, leading to the disruption of dispersion stability. Control experiments were conducted and are presented in Figure 2d. Under dark conditions, no products were detected, indicating that H_2O_2 and glycerol cannot react over 0.25Cu/WO_3 without light irradiation. Similarly, in the absence of the catalyst, no products were observed. Therefore, it can be concluded that the photocatalysis process is the sole contributor to glycerol conversion.

To unravel the mechanism behind the high conversion rate and selectivity toward valuable glyceraldehyde and dihydroxyacetone over $Cu^{\delta+}$-decorated WO_3, W 4f and Cu 2p XPS spectra with and without light irradiation were recorded under dark and visible light conditions. Under dark conditions, the W 4f XPS spectrum presents three peaks at 41.5 eV, 37.9 eV and 35.7 eV, corresponding to the W $5p_{3/2}$, W $4f_{5/2}$ and W $4f_{7/2}$, respectively (Figure 3a). These peaks can be assigned to W^{6+}, indicating that WO_3 is predominantly composed of W^{6+} species. Under visible light irradiation, new peaks attributed to W^{5+} and W^{4+} emerge, indicating the reduction of a portion of W^{6+} species to lower oxidation states. These results align with previous observations reporting an increase in the amount of W^{5+} in WO_3 under light irradiation.[22] Regarding Cu species under visible light illumination, a clear positive shift of 0.4 eV and 0.5 eV is evident for Cu 2p3/2 and Cu 2p1/2, respectively. This shift implies the ongoing oxidation of specific Cu species, as illustrated in Figure 3b. By combining the W 4f and Cu 2p XPS results with and without light irradiation, the spatial

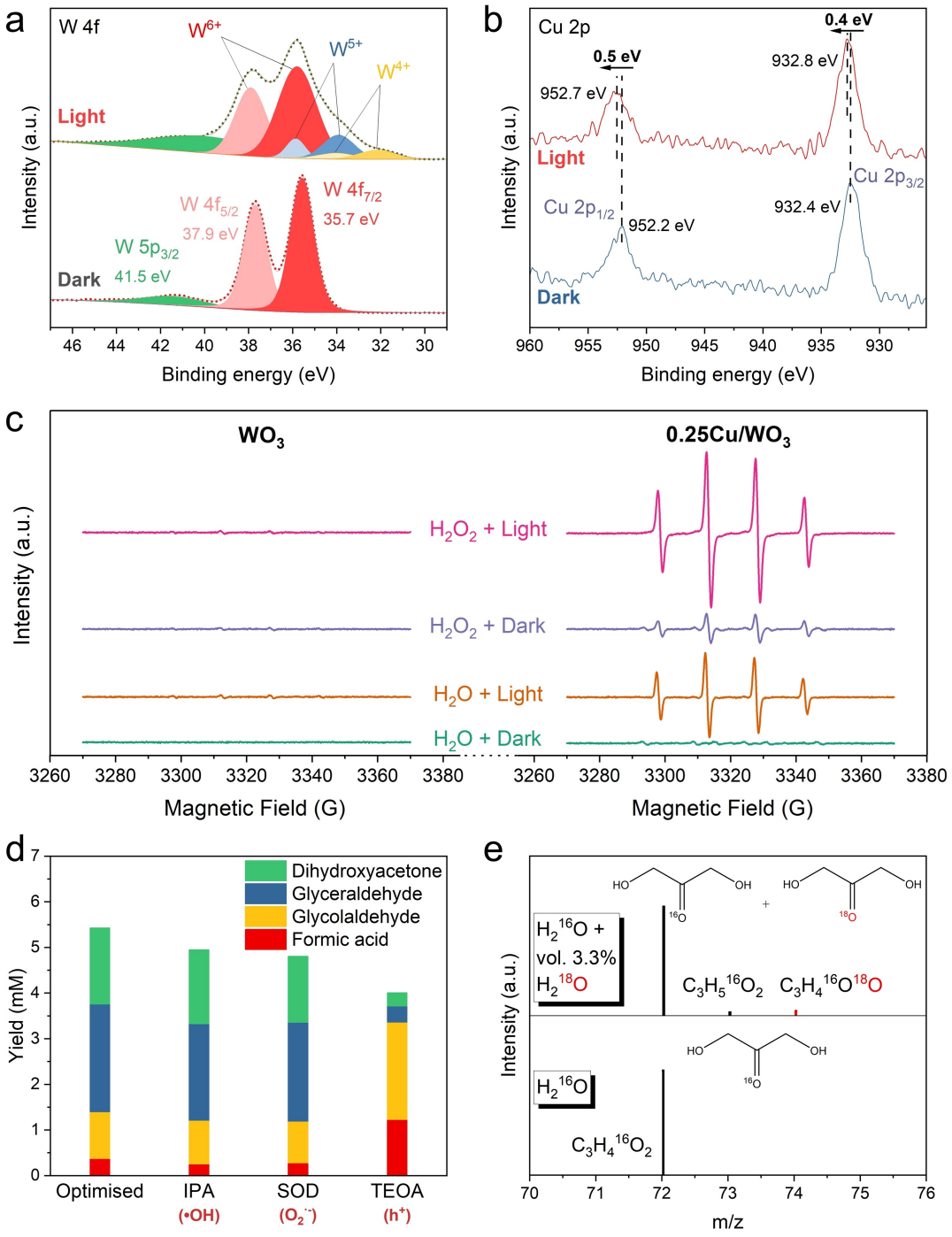

Figure 3. (a) W 4f XPS spectra of 0.25Cu/WO_3 in the dark and under visible light irradiation (>420 nm). (b) Cu 2p XPS spectra of 0.25Cu/WO_3 in the dark and under visible light irradiation (>420 nm). (c) ESR spectra for the detection of •OH on WO_3 and 0.25Cu/WO_3 under different conditions. (d) Product yields on 0.25Cu/WO_3 with the presence of different scavengers. (e) Isotope-labelled mass spectrum (m/z = 70–76) of liquid products under the same conditions using $H_2{}^{16}O$ or 3.3% vol. $H_2{}^{18}O$ in $H_2{}^{16}O$ as the reaction medium.

separation of charge carriers can be unambiguously elucidated—photogenerated electrons are trapped by $W^{\delta+}$ species in WO_3, while holes are transferred to $Cu^{\delta+}$ species.

To elucidate the glycerol oxidation mechanism over Cu/WO_3 and the involvement of H_2O_2 as the oxidant, studying the reaction Scheme is crucial. H_2O_2 can serve as an electron scavenger by undergoing the reduction reaction and generating •OH radicals, which might participate in the oxidation of glycerol. In order to detect the generated •OH over WO_3 and 0.25Cu/WO_3, electron spin resonance (ESR) spectroscopy was conducted. In the ESR spectrum of WO_3, regardless of the presence of H_2O_2, no distinct signals associated with •OH radicals were observed under both dark and visible light conditions (Figure 3c). This suggests that

pristine WO_3 lacks the capability to oxidise H_2O or reduce (decompose) H_2O_2 into •OH radicals. For 0.25Cu/WO_3, even under dark conditions, the addition of H_2O_2 resulted in a 1:2:2:1 quartet ESR signal, suggesting the facile generation of •OH. The decomposition of H_2O_2 into •OH radicals could readily take place with the catalysis of Cu species.[23] However, as illustrated in Figure 2d, no oxidation products are detected under dark conditions even in the presence of H_2O_2, eliminating the possibility that •OH radicals are responsible for glycerol oxidation. Under light irradiation, 0.25Cu/WO_3 showed a strong •OH-derived ESR signal, indicating enhanced charge transfer that accelerates the oxidative reaction. Upon adding H_2O_2, the •OH-derived ESR signal became even stronger, confirming the improved charge separation and validating the role of H_2O_2 as an electron scavenger.

To further investigate the involvement of photogenerated holes in the reaction with glycerol, scavenging experiments were conducted. These experiments aimed to identify the role of various reaction species potentially participating in the reaction. Isopropyl alcohol (IPA), superoxide dismutase (SOD), and triethanolamine (TEOA) were added to the reaction solution to selectively remove •OH, $O_2^{\bullet-}$, and h^+, respectively. The results in Figure 3d show that the addition of IPA and SOD had little impact on glycerol oxidation, indicating that •OH radicals and O2•⁻ do not play a significant role in the reaction. However, the addition of TEOA significantly altered the product distribution. Instead of glyceraldehyde and dihydroxyacetone, formic acid and glycolaldehyde became the major products. This finding confirms that the oxidation of glycerol to glyceraldehyde and dihydroxyacetone is directly initiated by photogenerated holes. When the catalyst is covered by TEOA, leading to hole scavenging, the primary reaction pathway shifts towards C–C cleavage. This alteration could be attributed to the generation of excessive •OH radicals in the reaction solution, which reacts with glycerol in the solution.

To delve further into the reaction pathway of glycerol oxidation over 0.25Cu/WO_3, an isotopic experiment was conducted using $H_2{}^{18}O$, as shown in Figure 3e. When the reaction medium contained $H_2{}^{18}O$ (vol. 3.3 %), gas chromatography–mass spectrometry results revealed that the detected dihydroxyacetone consisted of 4.0 % $C_3H_6{}^{16}O_2{}^{18}O$ and 96.0 % $C_3H_6{}^{16}O_3$, indicating that H_2O is the major source of oxygen for the C=O bond in dihydroxyacetone.

The 0.25Cu/WO_3 was subjected 16 h reaction over which time its activity decreased by approximately 54 % (Figure S12). To investigate the cause of this deactivation, the used catalyst was analysed by ICP-AES, XRD, UV/Vis and XPS spectroscopy (Table S1 and Figure S13, 14). The results obtained from ICP-AES revealed a 66.7 % loss of Cu species from the catalyst into the reaction solution. UV/Vis and XPS spectra displayed minimal changes, except for a reduction in the intensity of the Cu 2p XPS signal. These findings suggest that the decrease in activity is primarily attributed to the loss of the loaded cocatalyst, a common issue encountered in photocatalysis.

Based on the above results, a proposed reaction mechanism for the selective oxidation of glycerol into glyceraldehyde and dihydroxyacetone over 0.25Cu/WO_3 is depicted in Scheme 1. Upon illumination, incident light leads to the excitation of electrons from the valence band to the conduction band of WO_3, as indicated by the W 4f XPS spectra under dark and visible light conditions. Photogenerated holes are then transferred to Cu^+ atoms, oxidising them into Cu^{2+} species (as observed in the Cu 2p XPS spectra). Electrons on WO_3 are subsequently captured by adsorbed H_2O_2, resulting in the formation of OH^- and •OH radicals. The •OH radicals could be further reduced into OH^- by photogenerated electrons, then generating water.[24] Concurrently, glycerol molecules undergo a reaction with holes on $Cu^{\delta+}$ species, generating corresponding radicals (A). These carbon radicals further react with holes and hydroxide derived from water, forming gem-diol intermediates (B), which are unstable in an acidic environment and dehydrated to yield dihydroxyacetone.[25] This process also applies to the formation of glyceraldehyde, wherein the terminal carbon of glycerol is activated by holes.

Conclusions

In summary, an effective strategy to enhance the WO_3 photocatalytic activity for the selective oxidation of glycerol

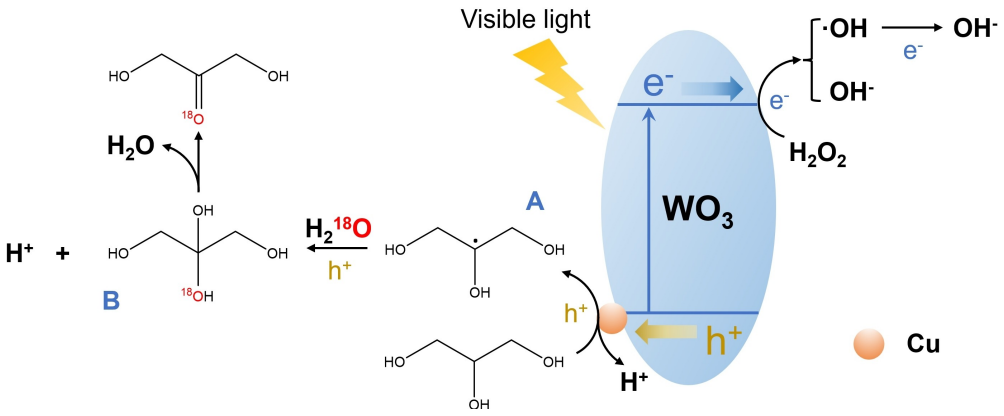

Scheme 1. Proposed reaction mechanism of glycerol oxidation on Cu-modified WO_3.

has been presented. The optimised catalyst, 0.25Cu/WO_3, consists of atomically dispersed $Cu^{\delta+}$ species on the WO_3 surface, as confirmed by EXAFS characterisation. Under visible light irradiation and in the presence of H_2O_2, the catalyst exhibits remarkable efficiency in converting glycerol into valuable trioses, glyceraldehyde and dihydroxyacetone, achieving a high conversion rate of 3.81 $mmol \cdot g^{-1} \cdot h^{-1}$ and sustained high selectivity towards both trioses. Through a comprehensive analysis involving various spectroscopies, scavenging experiments and isotopic analysis, the key factors contributing to the enhanced conversion rate and high selectivity under visible light and ambient conditions have been elucidated. The presence of Cu^+ species on the catalyst surface plays a crucial role by effectively attracting photogenerated holes, thereby improving charge transfer processes, then activating glycerol molecules by photogenerated holes over the Cu^+ species. This leads to the formation of corresponding carbon radicals, which subsequently couple with OH^- and undergo dehydration to yield the target products. The success of this strategy provides a valuable design protocol for enhancing the activity and controlling the selectivity of photocatalytic reactions.

Acknowledgements

We acknowledge the NSFC project (Grant No: 22250710677) and Beijing Municipal Project (C2022007). The work is also supported by Tsinghua University Initiative Scientific Research Program and UK EPSRC (EP/S018204/2). Z. Y., H. C., W. G., Y. S., X. P., L. Z., X. L., and A. W. are thankful for financial support from the National Natural Science Foundation of China (22132006, 21878289, 22172159) and CAS Project for Young Scientists in Basic Research (YSBR-022).

Conflict of Interest

The authors declare no conflict of interest.

Data Availability Statement

The data that support the findings of this study are available from the corresponding author upon reasonable request.

[1] L. R. Smith, M. Douthwaite, K. Mugford, N. F. Dummer, D. J. Willock, G. J. Hutchings, S. H. Taylor, in *Energies*, *Vol. 15*, **2022**.
[2] C.-H. Zhou, J. N. Beltramini, Y.-X. Fan, G. Q. Lu, *Chem. Soc. Rev.* **2008**, *37*, 527–549.
[3] P. M. Walgode, R. P. V. Faria, A. E. Rodrigues, *Catal. Rev.* **2021**, *63*, 422–511.
[4] a) D. Liu, J.-C. Liu, W. Cai, J. Ma, H. B. Yang, H. Xiao, J. Li, Y. Xiong, Y. Huang, B. Liu, *Nat. Commun.* **2019**, *10*, 1779; b) Y. Shen, A. Mamakhel, X. Liu, T. W. Hansen, T. Tabanelli, D. Bonincontro, B. B. Iversen, L. Prati, Y. Li, J. W. H. Niemantsverdriet, G. Hutchings, N. Dimitratos, A. Villa, R. Su, *J. Phys. Chem. C* **2019**, *123*, 19734–19741; c) L. Abis, N. Dimitratos, M. Sankar, S. J. Freakley, G. J. Hutchings, *Catal. Lett.* **2020**, *150*, 49–55; d) C. Liu, M. Hirohara, T. Maekawa, R. Chang, T. Hayashi, C.-Y. Chiang, *Appl. Catal. B* **2020**, *265*, 118543; e) J. Zhou, J. Hu, X. Zhang, J. Li, K. Jiang, Y. Liu, G. Zhao, X. Wang, H. Chu, *J. Catal.* **2020**, *381*, 434–442; f) H. Yan, Q. Shen, Y. Sun, S. Zhao, R. Lu, M. Gong, Y. Liu, X. Zhou, X. Jin, X. Feng, X. Chen, D. Chen, C. Yang, *ACS Catal.* **2021**, 6371–6383.
[5] S. T. Wu, Q. M. She, R. Tesser, M. D. Serio, C. H. Zhou, *Catal. Rev.* **2020**, 1–43.
[6] A. Behr, J. Eilting, K. Irawadi, J. Leschinski, F. Lindner, *Green Chem.* **2008**, *10*, 13–30.
[7] a) R. Ciriminna, G. Palmisano, C. D. Pina, M. Rossi, M. Pagliaro, *Tetrahedron Lett.* **2006**, *47*, 6993–6995; b) X. Ning, Y. Li, H. Yu, F. Peng, H. Wang, Y. Yang, *J. Catal.* **2016**, *335*, 95–104; c) Y. Kwon, Y. Birdja, I. Spanos, P. Rodriguez, M. T. M. Koper, *ACS Catal.* **2012**, *2*, 759–764; d) S. Schünemann, G. Dodekatos, H. Tüysüz, *Chem. Mater.* **2015**, *27*, 7743–7750; e) A. C. Garcia, M. J. Kolb, C. van Nierop y Sanchez, J. Vos, Y. Y. Birdja, Y. Kwon, G. Tremiliosi-Filho, M. T. M. Koper, *ACS Catal.* **2016**, *6*, 4491–4500.
[8] L. Xiong, J. Tang, *Adv. Energy Mater.* **2021**, *11*, 2003216.
[9] V. Maurino, A. Bedini, M. Minella, F. Rubertelli, E. Pelizzetti, C. Minero, in *Journal of Advanced Oxidation Technologies*, *Vol. 11*, **2008**, p. 184.
[10] a) P. Panagiotopoulou, E. E. Karamerou, D. I. Kondarides, *Catal. Today* **2013**, *209*, 91–98; b) M. de Oliveira Melo, L. A. Silva, *J. Photochem. Photobiol. A* **2011**, *226*, 36–41.
[11] V. Augugliaro, H. A. H. El Nazer, V. Loddo, A. Mele, G. Palmisano, L. Palmisano, S. Yurdakal, *Catal. Today* **2010**, *151*, 21–28.
[12] Y. Wang, H. Suzuki, J. Xie, O. Tomita, D. J. Martin, M. Higashi, D. Kong, R. Abe, J. Tang, *Chem. Rev.* **2018**, *118*, 5201–5241.
[13] X. Liu, H. Zhai, P. Wang, Q. Zhang, Z. Wang, Y. Liu, Y. Dai, B. Huang, X. Qin, X. Zhang, *Catal. Sci. Technol.* **2019**, *9*, 652–658.
[14] M. Stelmachowski, M. Marchwicka, E. Grabowska, M. Diak, **2014**, *17*, 167–178.
[15] Z. Chen, Y. Peng, F. Liu, Z. Le, J. Zhu, G. Shen, D. Zhang, M. Wen, S. Xiao, C.-P. Liu, Y. Lu, H. Li, *Nano Lett.* **2015**, *15*, 6802–6808.
[16] J. Yu, F. Dappozze, J. Martín-Gomez, J. Hidalgo-Carrillo, A. Marinas, P. Vernoux, A. Caravaca, C. Guillard, *Appl. Catal. B* **2021**, *299*, 120616.
[17] Z. H. Zhang, P. Wang, *J. Mater. Chem.* **2012**, *22*, 2456–2464.
[18] L. Xiong, H. Qi, S. Zhang, L. Zhang, X. Liu, A. Wang, J. Tang, *Advanced Materials* **2023**, *35*, 2209646.
[19] L. Yang, Y. Jiang, Z. Zhu, Z. Hou, *Molecular Catalysis* **2022**, *523*, 111545.
[20] M. Teranishi, S.-I. Naya, H. Tada, *J. Phys. Chem. C* **2016**, *120*, 1083–1088.
[21] C.-J. Chen, D.-H. Chen, *Nanoscale Res. Lett.* **2013**, *8*, 57.
[22] Y. Liu, X. Zeng, C. D. Easton, Q. Li, Y. Xia, Y. Yin, X. Hu, J. Hu, D. Xia, D. T. McCarthy, A. Deletic, C. Sun, J. Yu, X. Zhang, *Nanoscale* **2020**, *12*, 8775–8784.
[23] P. Pędziwiatr, F. Mikołajczyk, D. Zawadzki, K. Mikołajczyk, A. Bedka, *Acta Innovations* **2018**, 45–52.
[24] Y. Nosaka, A. Y. Nosaka, *Chem. Rev.* **2017**, *117*, 11302–11336.
[25] L. Luo, W. Chen, S.-M. Xu, J. Yang, M. Li, H. Zhou, M. Xu, M. Shao, X. Kong, Z. Li, H. Duan, *J. Am. Chem. Soc.* **2022**, *144*, 7720–7730.

Manuscript received: December 1, 2023
Accepted manuscript online: February 1, 2024
Version of record online: ■■, ■■

Communications

Heterogeneous Catalysis

L. Xiong, Z. Yu, H. Cao, W. Guan, Y. Su, X. Pan, L. Zhang, X. Liu, A. Wang,* J. Tang* — **e202318461**

Converting Glycerol into Valuable Trioses by $Cu^{\delta+}$-Single-Atom-Decorated WO_3 under Visible Light

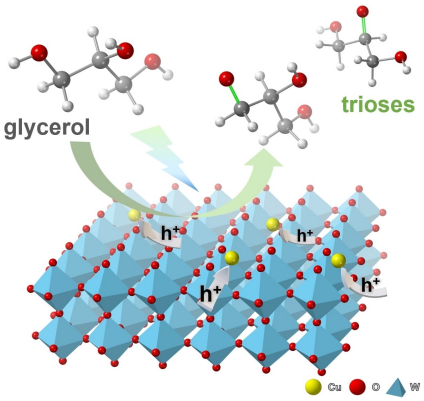

A single-atom Cu-decorated WO_3 photocatalyst has achieved a high conversion rate and excellent selectivity in the process of visible light-driven oxidation of glycerol to trioses. The critical role of single Cu atoms is to attract photogenerated holes, thereby improving charge transfer and activating glycerol molecules.